Dalton Transactions

ROYAL SOCIETY OF CHEMISTRY

PAPER

View Article Online
View Journal | View Issue

Check for updates

Cite this: *Dalton Trans.*, 2022, **51**, 11040

Excellent yield of a variety of silicon-boron radicals and their reactivity†

Mohd Nazish,[a] Yi Ding,[a] Christina M. Legendre,[a] Arun Kumar,[a] Nico Graw,[a] Brigitte Schwederski,[b] Regine Herbst-Irmer,[a] Parameswaran Parvathy,[c] Pattiyil Parameswaran,*[c] Dietmar Stalke,*[a] Wolfgang Kaim*[b] and Herbert W. Roesky*[a]

Received 27th April 2022,
Accepted 1st June 2022

DOI: 10.1039/d2dt01318e

rsc.li/dalton

Herein we report stable silicon-boron radicals of composition LSi(NMe$_2$)–B(Br)Tip (**1**), LSi(NMe$_2$)–B(I)Tip (**2**) LSi(^{t}Bu)–B(I)Tip (**3**) [L = PhC(N^{t}Bu)$_2$]. They were prepared in high yield using a one pot reaction of LSiR, X$_2$BTip and KC$_8$ in a 1 : 1 : 1 molar ratio (R = ^{t}Bu, NMe$_2$; X = Br, I). The reaction of the silicon–boron radical with Br$_2$ and Se affords the dihalogenated compound LSi(^{t}Bu)–B(Br$_2$)Tip (**4**) and oxidative addition product LSi(^{t}Bu)=Se (**5**). All the compounds were characterized by single-crystal X-ray structural analysis, electron paramagnetic resonance (EPR) analysis, elemental analysis, multinuclear NMR spectroscopy, and mass spectrometry. Quantum chemical calculations show that the B-centered radicals **1–3** are stabilised by hyperconjugative interactions.

Introduction

Compounds with low-valence silicon are heavily investigated for their high reactivity but challenging to obtain due to their very short lifetimes at ambient temperature. For many decades, silylenes have been considered to be short-lived species, either in the gas phase, in solution, or when trapped in frozen matrices.[1,2] The silicon atom possesses both a nucleophilic and an electrophilic reactive site. These can be modelled as a high energy-lying lone pair orbital and as a low energy lying vacant pπ orbital, respectively.[3] The isolation of the first stable silicon N-heterocyclic silylene (NHSi), analogous to Arduengo's N-heterocyclic carbene, was reported in 1994.[4,5] Such compounds display a two-coordinate Si(II) center with one empty p-orbital and one electron pair, indicative of their electron acceptor and donor characteristics. Another important compound with a low-valence silicon is the amidinate-supported[6] silylene LSiR (L = PhC(N^{t}Bu)$_2$; R = halide or organic group).[7] In comparison with NHSi, the silicon atom in LSiR is *N*,*N*′ chelated by both nitrogen atoms of the anionic ligand. This type of silylene is comparable to the acyclic silylene and represents a promising candidate for small molecule activation with unique reactivity and reaction patterns. Indeed, such reactions with LSiR were well studied with alkynes,[8,9] chalcogens[10] ketones,[11] CO,[12] and P$_4$.[13] The formation of adducts with boron compounds is usually obtained when LSiR reacts with a boron species, for example BH$_3$, 9-BBN, or B(C$_6$F$_5$)$_3$.[14] Surprisingly, the reactivity of the amidinate silylene (PhC(N^{t}Bu)$_2$SiCl) with boron compounds to synthesize silicon-boron radicals remained nearly unexplored.[15] It is noteworthy that N-heterocyclic carbenes (NHC), silylenes, and cyclic alkyl amino carbenes (cAAC) have been employed as effective bases to stabilize neutral boryl radicals.[16,17] In a previous publication, we have demonstrated and exploited the strong σ-donor and π-acceptor properties of cyclic alkyl(amino) carbenes (cAACs) for the stabilization of radical cations and radical anions of p-block elements.[18] Encouraged by this study, we focused on the synthesis of silicon-boron radicals with a variety of interesting substituents. Herein, we report the synthesis of high yield radicals and facile reduction of X$_2$BTip in the presence of LSiR, yielding three novel radical species LSi(NMe$_2$)–B(Br)Tip (**1**), LSi(NMe$_2$)–B(I)Tip (**2**) LSi(^{t}Bu)–B(I)Tip (**3**) [L = PhC(N^{t}Bu)$_2$]. The subsequent reactions of the obtained radicals with Br$_2$ give the disubstituted bromine compound LSi(^{t}Bu)–B(Br)Tip (**4**), while the addition of pure selenium results in decomposition, yielding a selenium–silicon compound LSi(^{t}Bu)=Se (**5**).

Results and discussion

The synthetic strategy of **1–3** involves the one-pot reaction of dibromo/iodo(2,4,6-triisopropylphenyl)borane with amidinate-silylene LSiNMe$_2$ and LSi^{t}Bu (L = PhC(N^{t}Bu)$_2$) and 1.0 equi-

[a]*Institut für Anorganische Chemie, Universität Göttingen, Tammannstrasse 4, Göttingen 37077, Germany. E-mail: hroesky@gwdg.de*
[b]*Institut für Anorganische Chemie, Universität Stuttgart, Pfaffenwaldring 55, Stuttgart 70569, Germany*
[c]*National Institute of Technology Calicut, Kozhikode, Kerala 673601, India*

†Electronic supplementary information (ESI) available: Synthetic, spectroscopic and structural data. CCDC 2113990–2113994. For ESI and crystallographic data in CIF or other electronic format see DOI: https://doi.org/10.1039/d2dt01318e

valent of potassium graphite. Diethyl ether was added at −78 °C and the reaction mixture was stirred overnight. Upon filtration of the solution under an inert atmosphere, the colorful clear solution was concentrated and stored at −30 °C. After one week, dark red or orange crystals of LSi(NMe_2)–B(Br)Tip (**1**), LSi(NMe_2)–B(I)Tip (**2**) and LSi(^{t}Bu)–B(I)Tip (**3**) were obtained, respectively, in 90%, 94% and 95% yields (Scheme 1).

The crystals were subsequently analyzed by single-crystal X-ray diffraction (Fig. 1–3). Compounds **1–3** crystallized in the monoclinic space group $P2_1/n$ with one molecule in the asymmetric unit. All three are similar in their overall geometry and feature a silicon–boron bond, as previously reported in analogous radical species.[15a]

The central silicon atom exhibits a distorted tetrahedral coordination environment due to the acute bite angle of the amidinate ligand. Additionally, the silicon atom is substituted by a NMe_2 (**1**, **2**) or ^{t}Bu (**3**) group and by a B(x)Tip substituent (**1**: X = Br, **2**, **3**: X = I). It is noteworthy that, in agreement with the increase of ionic radii, the B1–Br1 distance (2.0247(19) Å) in **1** is shorter than the B1–I1 distance (2.221(5) Å) in the analogous complex **2**. The boron atom shows an almost perfect trigonal planar environment with the sum of angles ranging between 359.69° and 359.98°. This should exclude the localization of the unpaired electron at the boron atom. The Si–B bond distances in **1–3** lie within the range of 1.916 Å to 1.930 Å which is on the shorter end of the reported Si–B single bonds (Fig. S22†) but very similar to that of the closely related

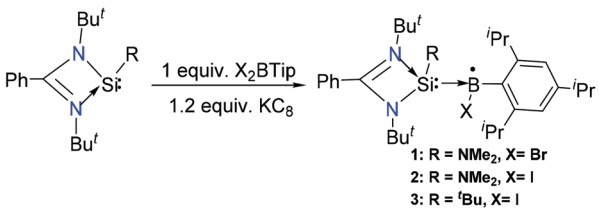

Scheme 1 Synthetic route for the synthesis of compounds **1–3**.

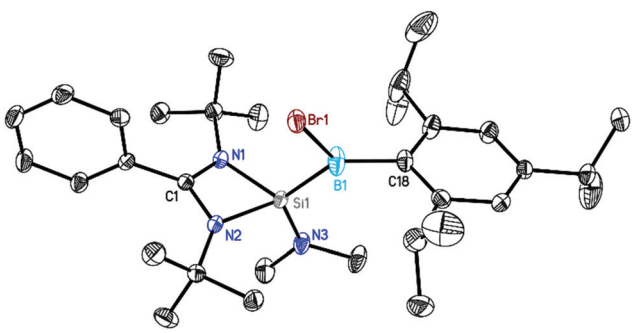

Fig. 1 Crystal structure of **1**. The anisotropic displacement parameters are depicted at the 50% probability level. Hydrogen atoms are omitted for clarity. Selected bond lengths [Å] and angles [°]: N1–Si1 1.8475(12), N2–Si1 1.8407(13), N3–Si1 1.6946(13), Si1–B1 1.9292(19), B1–Br1 2.0247(19), B1–C18 1.590(2), N1–Si1–N2 70.86(6), N1–Si1–B1 118.41(7), B1–Si1–N3 119.56(7), Br1–B1–Si1 109.47(9).

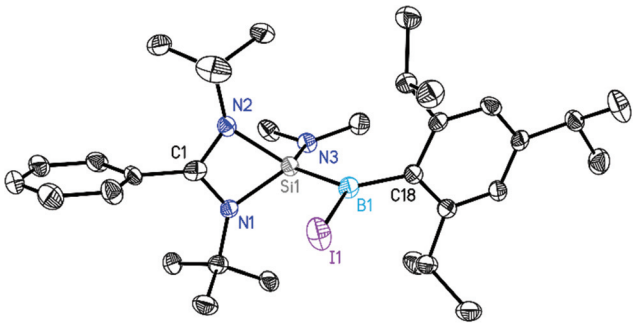

Fig. 2 Crystal structure of **2**. The anisotropic displacement parameters are depicted at the 50% probability level. Hydrogen atoms are omitted for clarity. Selected bond lengths [Å] and angles [°]: N1–Si1 1.818(4), N2–Si1 1.877(5), N3–Si1 1.700(3), Si1–B1 1.930(5), B1–I1 2.221(5), B1–C18 1.573(6), N1–Si1–N2 70.66(16), N1–Si1–B1 119.9(2), B1–Si1–N3 119.2(2), I1–B1–Si1 114.6(2).

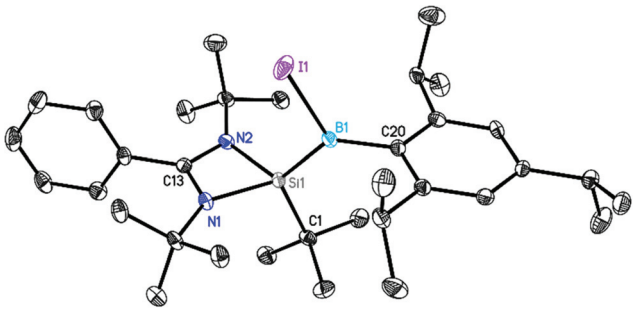

Fig. 3 Crystal structure of **3**. The anisotropic displacement parameters are depicted at the 50% probability level. Hydrogen atoms are omitted for clarity. Selected bond lengths [Å] and angles [°]: N1–Si1 1.852(3), N2–Si1 1.854(2), C1–Si1 1.906(2), Si1–B1 1.916(3), B1–I1 2.227(2), B1–C20 1.590(3), N1–Si1–N2 70.92(10), N1–Si1–B1 119.52(12), B1–Si1–C1 118.78(11), I1–B1–Si1 112.83(11).

radical compounds [LSi(^{t}Bu)–B(Br)Tip] (1.9136(14) Å)[15a] and [LSi(HMDS)–B(Br)Tip] (1.9641(19) Å).[15a]

The formation of radicals **1**, **2** and **3** was further confirmed by electron paramagnetic resonance spectroscopy and LIFDI mass spectrometry. Compound **1** exhibits an EPR spectrum at g = 2.0083 with a clearly resolved boron coupling of 14.9 Gauss (^{11}B, I = 3/2, 80.1% nat. abundance), signifying considerable spin density at B (Fig. 4). The iodine analogue **2** shows an unresolved EPR signal at 2.0028; the lack of resolution is attributed to slowed down mobility and increased spin orbit coupling involving the heavier element iodine. Compound **3** shows only partial EPR resolution (Fig. S1 and 2†). The LIFDI mass spectra in toluene solutions of **1**, **2** and **3** show ions at m/z, 598.5, 516.9, and 657.3, respectively, corresponding to the formation of [LSi(NMe_2)–B(Br)Tip], [LSi(NMe_2)–B(I)Tip], and [LSi(^{t}Bu)–B(I)Tip] (Fig. S10–12†). Compounds **1** and **2** have a melting point in the range of 205–215 °C whereas **3** melts at 200–205 °C, as determined by differential scanning calorimetry. Moreover, NMR spectroscopy shows the absence of the resultant resonance, due to the radical formation. Quantum

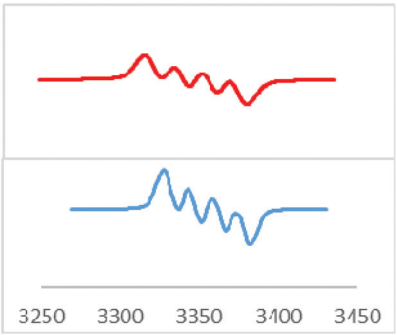

Fig. 4 EPR spectrum of **1** (bottom) with simulation (top) using a ^{11}B coupling constant of 14.9 G.

chemical calculations were carried out to explore the nature of the radical in compounds **1–3** at the M062X/def2-TZVPP//PBE/def2-TZVPP level of theory.[19] The structural parameters in the optimized geometries showed good agreement with the experimental geometries (Fig. S23†). All three compounds feature a trigonal planar B centre coordinated to an *N*-amidinate silylene, a Tip group and a halogen atom X (X = Br in **1**, I in **2** and **3**). The molecular orbital (MO) analysis reveals that the singly occupied molecular orbital (SOMO) in compounds **1–3** is a π-type p-orbital largely localized on the B centre (Fig. 5a). The frontier MOs of compounds **2** and **3** are similar to those in **1** (Fig. S24†). Bond orbital analysis within the NBO framework shows 0.71 − 0.76 electron occupancy on the p-type orbital (99.7%-p character) on the B center.

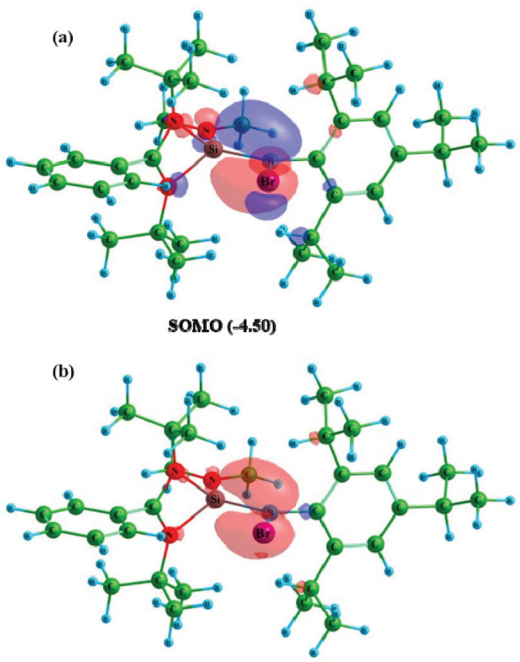

Fig. 5 Plot of (a) SOMO and (b) spin density of compound **1**. Isosurface value for MO and spin density is 0.05 and 0.0045 respectively. The eigenvalue of the SOMO is given in parenthesis in eV.

The spin density plot (Fig. 5b) reaffirms the above observation. The natural spin density on B is 0.73 in **1**, 0.75 in **2** and 0.70 in **3**. The NHC and cAAC stabilized B-centred radical compounds showed spin density in the range of 0.41 − 0.50 at the B atom.[20] Similar radical compounds LSi(L′)–B(Br)Tip (L′ = ^{t}Bu (**1**); N(TMS)$_2$ (**2**)) reported previously have 64 − 70% spin density on the B centre.[15] This indicates that although the spin is largely localized on the B centre, a significant part of the spin density is delocalized onto the adjacent ligand framework through hyperconjugative interactions. The *N*-amidinate silylene and the Tip group act as radical sinks, stabilizing these B-centered radical compounds. This is supported by natural spin density values on the Si (0.14 − 0.21), N1 (0.02), and N2 (0.02) centres and Tip (0.03 − 0.04) group.

Second-order perturbation analysis indicates that the B radical centre is stabilized by hyperconjugative interactions with the Si–N and C–C skeleton of the *N*-amidinate ligand and Tip ring, respectively. The strength of the donation from the B radical centre to the Si–N σ*-orbitals is 28.13 kcal mol^{-1} for **1**, 27.52 kcal mol^{-1} for **2** and 30.71 kcal mol^{-1} for **3**. The extent of hyperconjugative donation from the B p-orbital to the C–C σ*-orbitals of the Tip ring is 13.42 kcal mol^{-1}, 14.19 kcal mol^{-1} and 12.84 kcal mol^{-1} for **1–3** respectively. In all compounds, the strength of hyperconjugative donation towards the *N*-amidinate ligand is greater than that towards the Tip ring.

It is evident from the spin density analysis that the effect of halogen atom X (X = Br in **1**, I in **2** and **3**) on the radical density distribution is marginal. In contrast, the effect of the substituent R on the Si centre (R = NMe$_2$ for **1** and **2**, ^{t}Bu for **3**) is pronounced. This is because in compounds **1** and **2**, the lone pair on the nitrogen atom of the NMe$_2$ group is involved in hyperconjugative donation to the Si–N σ*-orbitals. Second-order perturbation analysis shows the strength of this donation to be 20.6 kcal mol^{-1} for **1** and 20.52 kcal mol^{-1} for **2**. This hyperconjugative interaction competes with the hyperconjugative interaction from the B p-type radical orbital, whereas in compound **3** with ^{t}Bu substitution, such an effect is absent. This results in more effective spin delocalization in compound **3** and in turn, a lower spin density value on B (0.70) in comparison with those of **1** and **2** (0.73 − 0.75). Topological analysis using the quantum theory of atoms in molecules indicates the polar covalent nature of the Si–B bond in compounds **1–3** (Fig. 6 and Fig. S27†).[19] The low value of electron density ($\rho(r)$ = 0.1213 − 0.1229 a.u) with negative values of Laplacian of electron density ($\nabla^2\rho(r)$ = −0.0495 to −0.0758 a.u) observed at the bond critical point (bcp) between the Si and B centres is characteristic of polar covalent interactions (Table 1 and Table S9†). This is also reflected in the respective positive and negative natural charges on the Si (1.79 − 1.86) and B (−0.29 to −0.33) centres (Table S7†). The ellipticity values (ε) in the range of 0.30 − 0.35 further support the back-bonding from the B centre to the Si centre in compounds **1–3**. Furthermore, the Si–B radical was characterized by cyclic voltammetry (all potentials are given *vs.* Fc$^{+/0}$). In dry and degassed acetonitrile, the Si–B radical undergoes an irreversible oxidation at E_{pa} = 0.32 V, as well as a quasi-reversible

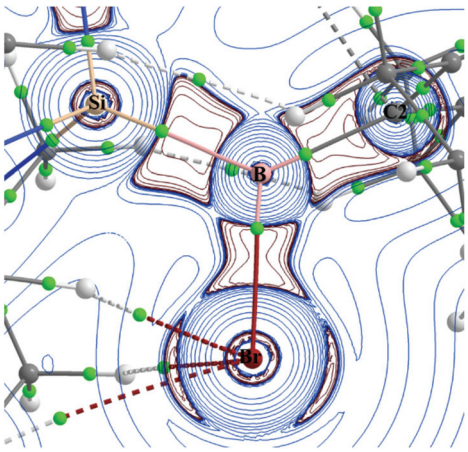

Fig. 6 Laplacian of electron density plotted in the Si–B–C2 plane of compound **1**. Bond critical points (green dots), areas of charge concentration (red; $\nabla^2\rho(r) < 0$), charge depletion (blue) and bond paths are represented.

Table 1 Topological parameters of electron density at the bond critical points of selected bonds in compound **1**. All values are in atomic units[a]

	Si–B	B–Br	B–C2
$\rho(r)$	0.1229	0.1000	0.1778
$\nabla^2\rho(r)$	−0.0758	−0.0757	−0.1841
$H(r)$	0.1120	0.1040	0.2370
$G(r)$	0.0738	0.0660	0.1445
$V(r)$	−0.1666	−0.1508	−0.3350
ε	0.35	0.11	0.03

[a] Electron density $\rho(r)$, Laplacian of electron density $\nabla^2\rho(r)$, energy density $H(r)$, Lagrangian kinetic energy $G(r)$, potential energy density $V(r)$, and ellipticity ε.

reduction at $E_{pc,1} = -1.34$ V with the respective oxidation of the reverse scan at $E_{pa,1} = -1.24$ V, and an irreversible reduction at $E_{pc,2} = -1.57$ V (Fig. 7; for full CV, see the ESI, Fig. S28†).

Our efforts began by exploring the reactivity of the Si–B radical with TEMPO and NO gas, but in both the reactions they showed a slow color change from red to light yellow at room temperature. However, we could not get clear NMR spectra and single-crystals for structural investigations. Furthermore the reactions of the Si–B radical with organic halides were studied but we could not observe any reactivity. Later on the Si–B radical resulted in oxidative addition products when we tried reactions with bromine and chalcogen (Se). Treatment of the silicon–boron radical with one equivalent of bromine in toluene at room temperature affords a yellow solution. The solution was further concentrated and stored at −30 °C in a freezer. After two weeks, yellow colored block-shaped crystals of dibrominated compound LSi(^{t}Bu)–B(Br_2)Tip (**4**), (68% isolated yield) were obtained from a concentrated solution (Scheme 2). In the reaction of compound **4**, we expected that the boron radical first generates the borenium cation (>B^+) by oxidation of the Si–B radical followed by the addition of a bromine anion (Br^-) to the borenium centre. The crystals of **4** were subsequently analyzed by single crystal X-ray diffraction (Fig. 8). Compound **4** crystallizes in the monoclinic space group $P2_1/n$ with one complex molecule in the asymmetric unit. The tetrahedral environment of the boron atom is distorted by the steric hindrances induced by the ^{t}Bu groups and the Tip ligand, resulting in angle variations between 96° (Br1–B1–Si1 angle) and 137° (C20–B1–Si1 angle). Compared to **1–3** and [LSi(^{t}Bu)–B(Br)Tip],[15a] the B–Si, B–C(Tip) and B–Br bond lengths are longer because of the fourfold silicon coordination in **4** compared to the threefold of the former.

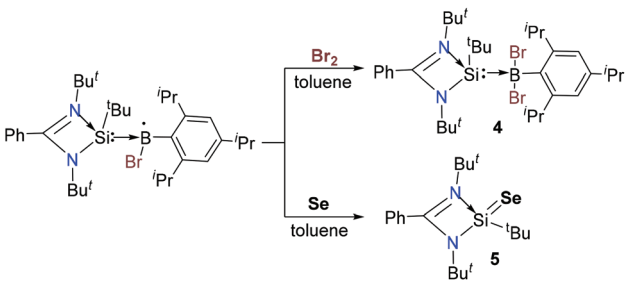

Scheme 2 Synthetic routes to **4** and **5**.

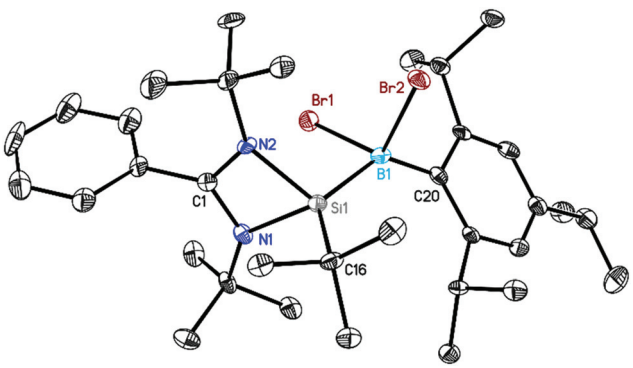

Fig. 8 Crystal structure of **4**. The anisotropic displacement parameters are depicted at the 50% probability level. Hydrogen atoms are omitted for clarity. Selected bond lengths [Å] and angles [°]: N1–Si1 1.826(4), N2–Si1 1.847(3), Si1–B1 2.096(4), B1–Br1 2.106(4), B1–Br2 2.090(3), B1–C20 1.627(5), N1–Si1–N2 71.85(12), N1–Si1–B1 113.87(13), B1–Si1–C16 133.22(14), Br1–B1–Si1 96.11(15), Br2–B1–Si1 98.95(15), C20–B1–Si1 137.0(2).

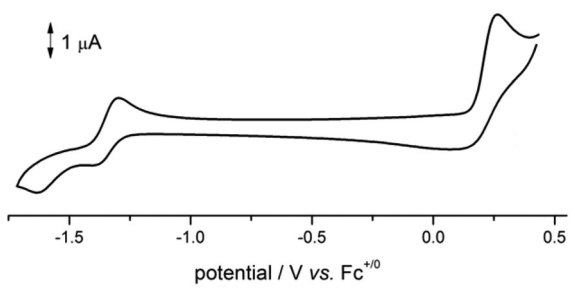

Fig. 7 Cyclic voltammetry of the Si–B radical.

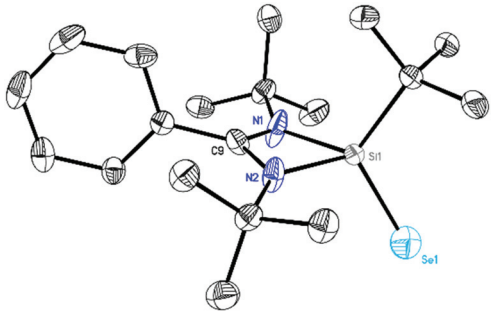

Fig. 9 Crystal structure of **5**. The anisotropic displacement parameters are depicted at the 50% probability level. Hydrogen atoms are omitted for clarity. Selected bond lengths [Å] and angles [°]: N1–Si1 1.8990(15), N2–Si1 1.8367(15), Si1–Se1 2.1394(17), N1–Si1–N2 72.24(6), N1–Si1–Se1 114.65(8).

LSi(^{t}Bu)=Se (**5**) was synthesized in 85% yield by reacting the Si–B radicals with one equivalent of selenium powder (Scheme 2). The color of the reaction mixture turned from red to light yellow. Product **5** was isolated as a colourless crystalline solid with good solubility in toluene. Subsequent analysis by single crystal X-ray diffraction reveals that the crystal contains two independent disordered molecules.

Compound **5** (Fig. 9) co-crystallizes in the monoclinic space group *C*2/*c* with the doubly protonated amidinate bromine salt and [L(H$_2$)Si(^{t}Bu)Br] and a toluene molecule (see ESI Fig. S19–21†). The central silicon atom in **5** is chelated by the amidinate ligand and coordinated by a ^{t}Bu group and a selenium atom. The Se1–Si1 bond is in the range of previously reported double bonds (2.1394(17) Å).[21] The formation of compounds **4** and **5** was further confirmed by ^{1}H, ^{13}C, ^{11}B and ^{29}Si NMR spectroscopy. The ^{29}Si NMR spectrum of **4** in C_6D_6 exhibits a resonance at δ −12.32 ppm for the Si(II) atoms, while compound **5** shows a signal in the ^{29}Si NMR spectrum at 36.21 ppm, both in good agreement with silicon II and IV complexes (Fig. S6 and S9†).[22]

The ^{1}H NMR spectra of **4** and **5** display sharp resonances for ^{t}Bu (δ 1.21 and 1.13 ppm) and for phenyl protons (δ 6.87–7.27 ppm) each, which is fully consistent with their solid-state molecular structures established by single-crystal X-ray diffraction (Fig. S3 and S7†). The ^{11}B NMR spectrum of **4** shows one resonance at δ −11.40 ppm which agrees with boron silicon adducts (Fig. S5†).[23] The formation of **4** and **5** was further confirmed by LIFDI mass spectrometry. They display their molecular ion in the mass spectrum at *m*/*z* 671.4 and 397.7, corresponding to the formation of LSi(^{t}Bu)–B(Br$_2$)Tip and LSi(^{t}Bu)=Se, (Fig. S13 and 14†). **4** and **5** have melting points at 225–230 °C and 215–222 °C, respectively, as determined by differential scanning calorimetry.

Conclusions

In conclusion, we report amidinate-supported divalent silicon atoms that are capable of stabilizing silicon-boron radicals in high to excellent yields with different substituents. Furthermore we also showed the reactivity of these radicals with bromine and selenium which led to the dihalogenation of boron (**4**) and the oxidative addition of selenium to silicon (**5**). All radicals **1**, **2** and **3** are highly stable at high temperatures in solution and towards air in the solid state. Quantum chemical calculations show that compounds **1–3** are primarily B-centred radical compounds that are stabilized *via* hyperconjugative interactions with the adjacent ligand framework. Compounds **4** and **5** are stable in solution and in the solid state under an inert atmosphere.

Experimental section

Materials and methods

Syntheses were carried out under an inert atmosphere of dinitrogen in oven-dried glassware using standard Schlenk techniques. All other manipulations were accomplished in a dinitrogen filled glove box. Solvents were purified by using an MBRAUN solvent purification system MB SPS-800. All chemicals were purchased from Aldrich and used without further purification. PhC(N^{t}Bu)$_2$Si(^{t}Bu)–B(Br)Tip was prepared as reported in the literature.[14] ^{1}H, ^{13}C, and ^{29}Si NMR spectra were recorded with a Bruker Avance DRX 500 spectrometer, using C_6D_6 as a solvent. Chemical shifts δ are given relative to SiMe$_4$. EI–MS spectra were obtained using a Finnigan MAT 8230 spectrometer. Elemental analyses were performed at the Institut für Anorganische Chemie, Universität Göttingen. For elemental analysis, the compounds were kept under vacuum for six hours to remove the solvent molecules. Melting points were measured in a sealed glass tube on a Büchi B-540 melting point apparatus.

Synthesis

PhC(N^{t}Bu)$_2$Si(NMe$_2$)–B(Br)Tip (1). To the mixture of LSiNMe$_2$ (303 mg, 1 mmol), Br$_2$BTip (376 mg, 1 mmol) and KC$_8$ (135 mg, 1 mmol), 40 mL of diethyl ether was added at −78 °C, in a 100 mL round bottom flask. The reaction mixture was allowed to warm to room temperature slowly to give a bluish-purple solution of compound **1** after 12 hours of stirring. The solution was filtered and concentrated to 10 mL under a low vacuum. The filtered solution was stored at −30 °C in a freezer. After one week dark red-orange block-shaped X-ray quality crystals of **1** were obtained from the concentrated solution of diethyl ether (yield: 536 mg, 90%). MP: 205–210 °C to an orange liquid. Elemental analysis (%) calcd for $C_{32}H_{52}BBrN_3Si$ (596.32): C, 64.32; H, 8.77; N, 7.03; found: C, 63.90; H, 9.02; N, 7.54. MS (LIFDI, toluene): *m*/*z* = 596.5 ([M]$^+$).

PhC(N^{t}Bu)$_2$Si(NMe$_2$)–B(I)Tip (2). To the mixture of LSiNMe$_2$ (303 mg, 1 mmol), I$_2$BTip (482 mg, 1 mmol) and KC$_8$ (135 mg, 1 mmol) 40 mL of diethyl ether was added at −78 °C, in a 100 mL round bottom flask. The reaction mixture was allowed to warm to room temperature slowly to give a bluish-purple solution of compound **2** after 12 hours of stirring. The solution

was filtered and concentrated to 10 mL under low vacuum. The filtered solution was stored at −30 °C in a freezer. After one week dark red-orange block-shaped X-ray quality crystals of **2** were obtained from the concentrated solution of diethyl ether (yield: 630 mg, 98%). MP: 205–210 °C to an orange liquid. Elemental analysis (%) calcd for $C_{32}H_{52}BBrN_3Si$ (644.31): C, 69.63; H, 8.13; N, 6.51; Found: C, 69.92; H, 8.72; N, 6.14. MS (LIFDI, toluene): m/z = 516.9 ($[M - I]^+$).

PhC(N^{t}Bu)$_2$Si(^{t}Bu)–B(I)Tip (3). A mixture of LSi^{t}Bu (318 mg, 1 mmol), I_2BTip (482 mg, 1 mmol) and KC_8 (135 mg, 1 mmol) was placed in a 100 mL round bottom flask, and 40 mL of diethyl ether was added at −78 °C. The reaction mixture was allowed to warm to room temperature slowly to give a reddish-purple solution of compound **3** after 12 hours of stirring. The solution was filtered and concentrated to 10 mL under a high vacuum. The filtered solution was stored at −30 °C in a freezer. After one week dark red-orange block-shaped X-ray quality crystals of **3** were obtained from the concentrated solution of diethyl ether (yield: 624 mg, 95%). MP: 210–215 °C to an orange liquid. Elemental analysis (%) calcd for $C_{34}H_{55}BIN_2Si$ (657.33): C, 62.10; H, 8.43; N, 4.26; found: C, 62.45; H, 8.92; N, 4.62. MS (LIFDI, toluene): m/z = 657.4 ($[M]^+$).

PhC(N^{t}Bu)$_2$Si(^{t}Bu)–B(Br$_2$)Tip (4). To the toluene solution of PhC(N^{t}Bu)$_2$Si(^{t}Bu)–B(Br)Tip (300 mg, 0.5 mmol), in a 50 mL round bottom flask, the Br_2 (80 mg, 0.5 mmol) solution in toluene was added dropwise at a low temperature. The reaction mixture was allowed to stir at room temperature to give a yellow-colored solution of compound **4** after 12 hours. The solution was evaporated under a high vacuum and extracted in diethyl ether and concentrated to 5 mL under a low vacuum. The filtered solution was stored at −30 °C in a freezer. After two weeks dark yellow block-shaped X-ray quality crystals of **4** were obtained from the concentrated solution of diethyl ether (yield: 234 mg, 68%). MP: 225–230 °C to a colorless liquid. ^{1}H NMR (500 MHz, C_6D_6, 298 K, ppm): δ = 1.21 (s, 18 H, C*Me3*), 1.33 (d, 6 H, CH*Me2*, J = 10 Hz), 1.48 (d, 6 H, CH*Me2*, J = 15 Hz), 1.53 (s, 9 H, C*Me3*), 1.70 (d, 6 H, CH*Me2*, J = 10 Hz), 2.97 (sep, 1 H, CH*Me2*), 3.47 (s, br, 2 H, CH*Me2*) 6.87–6.90 (m, 4 H, Ar*H*), 6.94–6.96 (m, 1 H, Ar*H*), 7.25–7.27 (m, 2 H, Ar*H*). ^{13}C NMR (126 MHz, C_6D_6, 298 K, ppm): δ = 23.96, 24.61, 26.08, 28.36, 31.97, 34.30, 34.73, 57.15, 66.24, 124.22, 128.71, 129.04, 129.85, 130.09, 130.11, 133.52, 151.35, 152.66, 183.52. ^{11}B NMR (160 MHz, C_6D_6, 298 K, ppm): δ = 11.40. ^{29}Si NMR (99 MHz, C_6D_6, 298 K, ppm): δ = −12.32. Elemental analysis (%) calcd for $C_{34}H_{55}BBr_2N_2Si$ (688.26): C, 59.14; H, 8.03; N, 4.06; found: C, 59.62; H, 8.60; N, 4.42. MS (LIFDI, toluene): m/z = 672.4 ($[M - CH4]^+$).

PhC(N^{t}Bu)$_2$Si(^{t}Bu)=Se (5). Toluene solution was added to the mixture of PhC(N^{t}Bu)$_2$Si(^{t}Bu)–B(Br)Tip (300 mg, 0.5 mmol) and Se powder (40 mg, 0.5 mmol) at room temperature in a 50 mL round bottom flask. The reaction mixture was allowed to stir overnight to give a yellow-colored solution of compound **5** after 20 h. The solution was filtered under a N_2 atmosphere and then the filtered solution was stored at room temperature. After one-month colorless block-shaped X-ray quality crystals of **5** were obtained from the concentrated solution of toluene (yield: 170 mg, 86%). MP: 225–230 °C to a colorless liquid. ^{1}H NMR (500 MHz, C_6D_6, 298 K, ppm): δ = 1.13 (s, 18 H, C*Me3*), 1.39 (s, 9 H, C*Me3*), 6.87–6.92 (m, 3 H, Ar*H*), 6.97–6.99 (m, 1 H, Ar*H*), 7.03–7.04 (m, 1 H, Ar*H*). ^{13}C NMR (126 MHz, C_6D_6, 298 K, ppm): δ = 24.02, 28.30, 31.84, 55.17, 128.06, 128.11, 128.16, 128.75, 130.48, 131.28, 175.28. ^{29}Si NMR (99 MHz, C_6D_6, 298 K, ppm): δ = 36.21, no signals could be observed in ^{77}Se NMR; elemental analysis (%) calcd for $C_{19}H_{32}N_2SeSi$ (396.15): C, 57.70; H, 8.16; N, 7.08; found: C, 58.07; H, 8.67; N, 7.53. MS (LIFDI, toluene): m/z = 397.7 ($[M]^+$).

Crystal structure determination

Crystals suitable for single crystal X-ray diffraction were mounted at a low temperature in inert oil under a nitrogen atmosphere by applying an X-Temp 2 device.[24] Diffraction data were collected at 100 K with a Bruker D8 three circle diffractometer equipped with an incoatec Mo Microsource (**1**, **3–5**) or a Bruker Mo rotating anode (**2**) with mirror optics (MoKα radiation, λ = 0.71073 Å). The data were integrated with SAINT[25] and an empirical absorption correction was applied with SADABS[26] (**1–2**, **4–5**) or TWINABS (**3**).[27] The structures were solved by SHELXT[28] and refined on F^2 using SHELXL[29] in the graphical user interface ShelXle.[30]

Crystal data for 1 at 100(2) K

$C_{32}H_{52}BBrN_3Si$, M_r = 597.57 g mol^{-1}, 0.359 × 0.337 × 0.201 mm, monoclinic, $P2_1/n$, a = 11.102(2) Å, b = 14.901(2) Å, c = 21.157(3) Å, β = 102.55(2), V = 3416.4(9) Å^3, Z = 4, μ (Mo Kα) = 1.262 mm^{-1}, θ_{max} = 28.413°, 133 144 reflections measured, 8563 independent (R_{int} = 0.0498), $R1$ = 0.0325 [$I > 2\sigma(I)$], w$R2$ = 0.0830 (all data), res. density peaks: 0.402 to −0.335 eÅ^3, CCDC 2113990.†

Crystal data for 2 at 100(2) K

$C_{32}H_{52}BIN_3Si$, M_r = 644.56 g mol^{-1}, 0.426 × 0.224 × 0.122 mm, monoclinic, $P2_1/n$, a = 12.626(2) Å, b = 18.594(3) Å, c = 14.454 (2) Å, β = 90.75(2), V = 3393.0(9) Å^3, Z = 4, μ (Mo Kα) = 1.003 mm^{-1}, θ_{max} = 25.171°, 126 965 reflections measured, 6038 independent (R_{int} = 0.0597), $R1$ = 0.0447 [$I > 2\sigma(I)$], w$R2$ = 0.0938 (all data), res. density peaks: 0.656 to −1.317 eÅ^3, CCDC 2113991.†

Crystal data for 3 at 100(2) K

$C_{34}H_{55}BIN_2Si$, M_r = 657.60 g mol^{-1}, 0.255 × 0.146 × 0.125 mm, monoclinic, $P2_1/n$, a = 12.623(2) Å, b = 19.291(3) Å, c = 14.451 (2) Å, β = 92.06(2), V = 3516.7(9) Å^3, Z = 4, μ (Mo Kα) = 0.968 mm^{-1}, θ_{max} = 29.284°, 70 008 reflections measured, 9573 independent (R_{int} = 0.0727), $R1$ = 0.0392 [$I > 2\sigma(I)$], w$R2$ = 0.0733 (all data), res. density peaks: 0.490 to −0.832 eÅ^3, CCDC 2113992.†

Crystal data for 4 at 100(2) K

$C_{34}H_{55}BBr_2N_2Si$, M_r = 690.52 g mol^{-1}, 0.276 × 0.231 × 0.127 mm, monoclinic, $P2_1/n$, a = 16.079(2) Å, b = 12.497(2) Å,

c = 17.886(3) Å, β = 106.12(2), V = 3452.7(11) Å^3, Z = 4, μ (Mo Kα) = 2.408 mm^{-1}, θ_{max} = 27.614°, 147 210 reflections measured, 7978 independent (R_{int} = 0.0832), $R1$ = 0.0448 [$I > 2\sigma(I)$], w$R2$ = 0.1226 (all data), res. density peaks: 2.088 to −1.235 eÅ^3, CCDC 2113993.†

Crystal data for 5 at 100(2) K

$C_{41}H_{65}BrSeSi$, M_r = 800.93 g mol^{-1}, 0.350 × 0.236 × 0.122 mm, monoclinic, $C2/c$, a = 30.532(3) Å, b = 8.760(2) Å, c = 18.768(2) Å, β = 122.67(2), V = 4225.2(14) Å^3, Z = 4, μ (Mo Kα) = 1.894 mm^{-1}, θ_{max} = 28.421°, 64 030 reflections measured, 5315 independent (R_{int} = 0.0409), $R1$ = 0.0234 [$I > 2\sigma(I)$], w$R2$ = 0.0544 (all data), res. density peaks: 0.354 to −0.331 eÅ^3, CCDC 2113994.†

Conflicts of interest

There are no conflicts to declare.

Acknowledgements

D. S. acknowledges partial funding from the Danish National Research Foundation (DNRF93) Center of Materials Crystallography. C. M. L. thanks the Fonds der Chemischen Industrie for financial support for her Ph.D. studies. We thank Dr A. C. Stückl for measuring the EPR spectrum. Parvathy thanks the NITC for the research fellowship and CCMS for computational facility. Dr Parameswaran thanks the DST-SERB for research funding.

Notes and references

1 P. P. Gaspar and R. West, ed. Z. Rappoport and Y. Apeloig, John Wiley and Sons, The Chemistry of Organic Silicon Compounds, Chichester, 1998, vol. 2, Part 3, pp. 2463–2567.
2 (*a*) M. Haaf, T. A. Schmedake and R. West, *Acc. Chem. Res.*, 2000, **33**, 704–714; (*b*) B. Gehrhus and M. F. Lappert, *J. Organomet. Chem.*, 2001, **618**, 209–223; (*c*) S. Yao, Y. Xiong and M. Driess, *Organometallics*, 2011, **30**, 1748–1767; (*d*) M. Kira, *Chem. Commun.*, 2010, **46**, 2893–2903; (*e*) R. Azhakar, R. S. Ghadwal, H. W. Roesky, H. Wolf and D. Stalke, *Chem. Commun.*, 2012, **48**, 4561–4563; (*f*) R. S. Ghadwal, R. Azhakar and H. W. Roesky, *Acc. Chem. Res.*, 2013, **46**, 444–456.
3 (*a*) R.-E. Li, J.-H. Sheu and M.-D. Su, *Inorg. Chem.*, 2007, **46**, 9245–9253; (*b*) P. W. Percival, J.-C. Brodovitch, M. Mozafari, A. Mitra, R. West, R. S. Ghadwal, R. Azhakar and H. W. Roesky, *Chem. – Eur. J.*, 2011, **17**, 11970–11973; (*c*) S. Inoue, J. D. Epping, E. Irran and M. Driess, *J. Am. Chem. Soc.*, 2011, **133**, 8514–8517; (*d*) S. Inoue, W. Wang, C. Präsang, M. Asay, E. Irran and M. Driess, *J. Am. Chem. Soc.*, 2011, **133**, 2868–2871; (*e*) R. S. Ghadwal, R. Azhakar, H. W. Roesky, K. Pröpper, B. Dittrich, C. Goedecke and G. Frenking, *Chem. Commun.*, 2012, **48**, 8186–8188.
4 P. Jutzi, D. Kanne and C. Krüger, *Angew. Chem., Int. Ed. Engl.*, 1986, **25**, 164.
5 M. Denk, R. Lennon, R. Hayashi, R. West, A. V. Belyakov, H. P. Verne, A. Haaland, M. Wagner and N. Metzler, *J. Am. Chem. Soc.*, 1994, **116**, 2691–2692.
6 D. Stalke, M. Wedler and F. T. Edelmann, *J. Organomet. Chem.*, 1992, **431**, C1–C5.
7 (*a*) S. S. Sen, H. W. Roesky, D. Stern, J. Henn and D. Stalke, *J. Am. Chem. Soc.*, 2010, **132**, 1123–1126.
8 (*a*) R. Azhakar, R. S. Ghadwal, H. W. Roesky, H. Wolf and D. Stalke, *Organometallics*, 2012, **31**, 4588–4592; (*b*) R. Azhakar, R. S. Ghadwal, H. W. Roesky, H. Wolf and D. Stalke, *Chem. Commun.*, 2012, **48**, 4561–4563.
9 S. S. Sen, H. W. Roesky, K. Meindl, D. Stern, J. Henn, A. C. Stückl and D. Stalke, *Chem. Commun.*, 2010, **46**, 5873–5875.
10 N. Parvin, S. Pal, S. Khan, S. Das, S. K. Pati and H. W. Roesky, *Inorg. Chem.*, 2017, **56**, 1706–1712.
11 R. S. Ghadwal, S. S. Sen, H. W. Roesky, M. Granitzka, D. Kratzert, S. Merkel and D. Stalke, *Angew. Chem., Int. Ed.*, 2010, **49**, 3952–3955.
12 Y. Wang, A. Kostenko, T. J. Hadlington, M.-T. Luecke, S. Yao and M. Driess, *J. Am. Chem. Soc.*, 2019, **141**, 626–634.
13 S. S. Sen, S. Khan, H. W. Roesky, D. Kratzert, K. Meindl, J. Henn, D. Stalke, J.-P. Demers and A. Lange, *Angew. Chem., Int. Ed.*, 2011, **50**, 2322–2325.
14 (*a*) A. Jana, D. Leusser, I. Objartel, H. W. Roesky and D. Stalke, *Dalton Trans.*, 2011, **40**, 5458–5463; (*b*) A. Jana, R. Azhakar, S. P. Sarish, P. P. Samuel, H. W. Roesky, C. Schulzke and D. Koley, *Eur. J. Inorg. Chem.*, 2011, **2011**, 5006–5013.
15 (*a*) M. Nazish, C. M. Legendre, S. K. Sarkar, J. Lücken, D. J. Goffitzer, M. Diefenbach, B. Schwederski, R. Herbst-Irmer, D. Stalke, M. C. Holthausen, W. Kaim and H. W. Roesky, *Inorg. Chem.*, 2021, **60**, 10100–10104.
16 (*a*) S. Ueng, A. Solovyev, X. Yuan, S. J. Geib, L. Fensterbank, E. Lacôte, M. Malacria, M. Newcomb, J. C. Walton and D. P. Curran, *J. Am. Chem. Soc.*, 2009, **131**, 11256–11262; (*b*) S. Ueng, M. M. Brahmi, E. Derat, L. Fensterbank, E. Lacôte, M. Malacria and D. P. Curran, *J. Am. Chem. Soc.*, 2008, **130**, 10082–10083; (*c*) P. Bissinger, H. Braunschweig, A. Damme, I. Krummenacher, A. K. Phukan, K. Radacki and S. Sugawara, *Angew. Chem., Int. Ed.*, 2014, **53**, 7360–7363; (*d*) F. Dahcheh, D. Martin, D. W. Stephan and G. Bertrand, *Angew. Chem.*, 2014, **126**, 13375–13379.
17 For selected reviews, see: (*a*) X. Bugaut and F. Glorius, *Chem. Soc. Rev.*, 2012, **41**, 3511–3522; (*b*) M. Soleilhavoup and G. Bertrand, *Acc. Chem. Res.*, 2015, **48**, 256–266; (*c*) F. E. Hahn and M. C. Jahnke, *Angew. Chem., Int. Ed.*, 2008, **47**, 3122–3172; (*d*) M. Melaimi, M. Soleilhavoup and G. Bertrand, *Angew. Chem., Int. Ed.*, 2010, **49**, 8810–8849; (*e*) M. Melaimi, R. Jazzar, M. Soleilhavoup and G. Bertrand, *Angew. Chem., Int. Ed.*, 2017, **56**, 10046–10068; (*f*) M. H. Wang and K. A. Scheidt, *Angew. Chem., Int. Ed.*, 2016, **55**, 14912–14922; (*g*) J. P. Moerdyk, D. Schilter and

C. W. Bielawski, *Acc. Chem. Res.*, 2016, **49**, 1458–1468; (*h*) C. D. Martin, M. Soleilhavoup and G. Bertrand, *Chem. Sci.*, 2013, **4**, 3020–3030.

18 (*a*) C. Mohapatra, S. Kundu, A. N. Paesch, R. Herbst-Irmer, D. Stalke, D. M. Andrada, G. Frenking and H. W. Roesky, *J. Am. Chem. Soc.*, 2016, **138**, 10429–10432; (*b*) S. Roy, K. C. Mondal and H. W. Roesky, *Acc. Chem. Res.*, 2016, **49**, 357–359; (*c*) B. Li, S. Kundu, A. C. Stückl, H. Zhu, H. Keil, R. Herbst-Irmer, D. Stalke, B. Schwederski, W. Kaim, D. M. Andrada, G. Frenking and H. W. Roesky, *Angew. Chem., Int. Ed.*, 2017, **56**, 397–400; (*d*) M. Melaimi, R. Jazzar, M. Soleilhavoup and G. Bertrand, *Angew. Chem., Int. Ed.*, 2017, **56**, 10046–10068; (*e*) S. Sinhababu, S. Kundu, A. N. Paesch, R. Herbst-Irmer, D. Stalke, I. Fernández, G. Frenking, A. C. Stückl, B. Schwederski, W. Kaim and H. W. Roesky, *Chem. – Eur. J.*, 2018, **24**, 1264–1268; (*f*) K. C. Mondal, H. W. Roesky, B. Dittrich, N. Holzmann, M. Hermann, G. Frenking and A. Meents, *J. Am. Chem. Soc.*, 2013, **135**, 15990–15993; (*g*) M. M. Siddiqui, S. K. Sarkar, M. Nazish, M. Morganti, C. Köhler, J. Cai, L. Zhao, R. Herbst-Irmer, D. Stalke, G. Frenking and H. W. Roesky, *J. Am. Chem. Soc.*, 2021, **143**, 1301–1306.

19 See ESI for computational details.†

20 (*a*) R. Kinjo, B. Donnadieu, M. C. Celik, G. Frenking and G. Bertrand, *Science*, 2011, **333**, 610–613; (*b*) M. F. S. Valverde, P. Schweyen, D. Gisinger, T. Bannenberg, M. Freytag, C. Kleeberg and M. Tamm, *Angew. Chem., Int. Ed.*, 2017, **56**, 1135–1140; (*c*) R. Bertermann, H. Braunschweig, R. D. Dewhurst, D. C. C. Hörl, D. C. T. Kramer and I. Krummenacher, *Angew. Chem., Int. Ed.*, 2014, **53**, 5453–5457.

21 (*a*) M. Ghosh, P. Panwaria, S. Tothadi, A. Das and S. Khan, *Inorg. Chem.*, 2020, **59**, 17811–17821; (*b*) M. Nazish, M. M. Siddiqui, S. K. Sarkar, A. Münch, C. M. Legendre, R. Herbst-Irmer, D. Stalke and H. W. Roesky, *Chem. – Eur. J.*, 2021, **27**, 1744–1752; (*c*) S.-H. Zhang, H.-X. Yeong and C.-W. So, *Chem. – Eur. J.*, 2011, **17**, 3490–3499.

22 S. Sinhababu, M. M. Siddiqui, S. K. Sarkar, A. Münch, R. Herbst-Irmer, A. George, P. Parameswaran, D. Stalke and H. W. Roesky, *Chem. – Eur. J.*, 2019, **25**, 11422–11426.

23 J. Li, Y. Liu, S. Kundu, H. Keil, H. Zhu, R. Herbst-Irmer, D. Stalke and H. W. Roesky, *Inorg. Chem.*, 2020, **59**, 7910–7914.

24 (*a*) T. Kottke and D. Stalke, *J. Appl. Crystallogr.*, 1993, **26**, 615–619; (*b*) D. Stalke, *Chem. Soc. Rev.*, 1998, **27**, 171–178.

25 Bruker AXS Inc., *Bruker Apex CCD, SAINT v8.37A*, Bruker AXS Inst. Inc., WI, USA, Madison, 2017.

26 L. Krause, R. Herbst-Irmer, G. M. Sheldrick and D. Stalke, *J. Appl. Crystallogr.*, 2015, **48**, 3–10.

27 M. Sevvana, M. Ruf, I. Usón, G. M. Sheldrick and R. Herbst-Irmer, *Acta Crystallogr., Sect. D: Struct. Biol.*, 2019, **75**, 1040–1050.

28 G. M. Sheldrick, *Acta Crystallogr., Sect. A: Found. Adv.*, 2015, **A71**, 3–8.

29 G. M. Sheldrick, *Acta Crystallogr., Sect. C: Struct. Chem.*, 2015, **C71**, 3–8.

30 C. B. Hübschle, G. M. Sheldrick and B. Dittrich, *J. Appl. Crystallogr.*, 2011, **44**, 1281–1284.